Supplementary Information

Divergent Phase Evolution in Mixed Oxide $W_{0.5}Mo_{0.5}O_3$ under Electron Beam Irradiation and Thermal Annealing

Naveen Goyal [a, b, *], Johannes Biskupek [b], Ute Kaiser [b, c, *]

[a]Collaborative Research Centre, Technical University Dresden, 01062, Germany

[b]Electron Microscopy Group of Materials Science, University of Ulm, 89081, Germany

[c]Institute of Quantum Optics, University of Ulm, 89081, Germany

*Corresponding Authors: naveen.goyal@mailbox.tu-dresden.de, ute.kaiser@uni-ulm.de

Computational details

The DFT calculations were performed using Vienna ab-initio simulation package (VASP) by considering spin polarization.[1] Mo_4O_{11} unit cell in orthorhombic crystal system and P_{nma} space group was taken from materials project database[2] and further, half of the Mo atoms were randomly substituted by W to obtain $Mo_2W_2O_{11}$. All electron projector-augmented wave (PAW)[3] pseudopotentials were used to describe the electron-ion interactions, wherein Mo ($4p^6\ 4d^5\ 5s^1$), W ($5p^6\ 5d^5\ 6s^1$) and O ($2s^2,2p^4$) shells were treated as valence shells. Electronic exchange and correlation were approximated by Perdew-Burke-Ernzerhof (PBE) functional under generalized gradient approximation (GGA).[4] The structural optimization was performed until the Hellman-Feynman forces acting on each atom were less than 0.01 eV/Å and the energy tolerance was set to 10^{-5} eV. The Brillouin zone for optimization of unit cells was sampled using a gamma centred 4x3x1 k-point grid. To account for strongly localized d-orbitals on transition metals, an on-site effective Hubbard (U-J = U_{eff}) parameter has been used, as introduced by Dudarev et. al. [5] The U_{eff} values for Mo and W were chosen as 4.4 and 6.2 eV, respectively. The formation energies for Mo_4O_{11} and $Mo_2W_2O_{11}$ were calculated from their optimized structures by using the equation below.

$$E_{formation} = E_{total} - n(Mo) * \mu(Mo) - n(W) * \mu(W) - n(O) * \mu(O)$$

The chemical potentials of Mo, W were calculated from their respective body centered cubic unit cells. The chemical potential for oxygen atoms was calculated as 1/2 μ (O_2 (g)).

Supplementary Figures

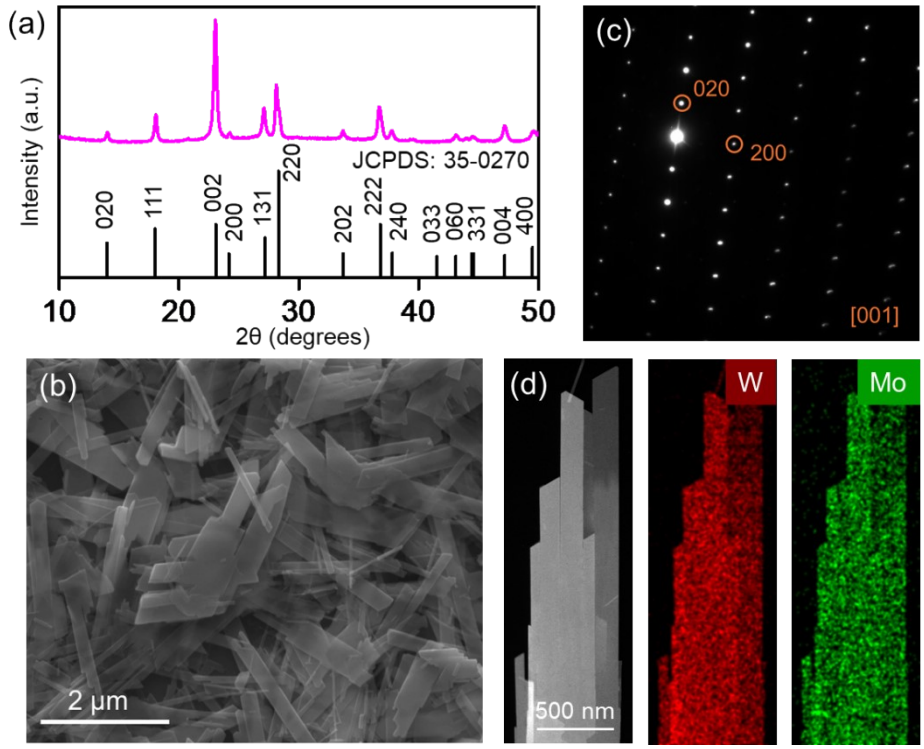

Fig. S1: Structural characterization of $W_{0.5}Mo_{0.5}O_3$; **(a)** PXRD pattern matching with orthorhombic phase of mixed metal oxide having composition $W_{0.5}Mo_{0.5}O_3\,0.33H_2O$; **(b)** SEM micrograph showing uniform belt-shaped morphology; **(c)** SAED pattern along [001] zone axis depicting single-crystalline nature; **(d)** STEM-EDS mapping showing uniform distribution of W and Mo with atomic fraction of 1:1.

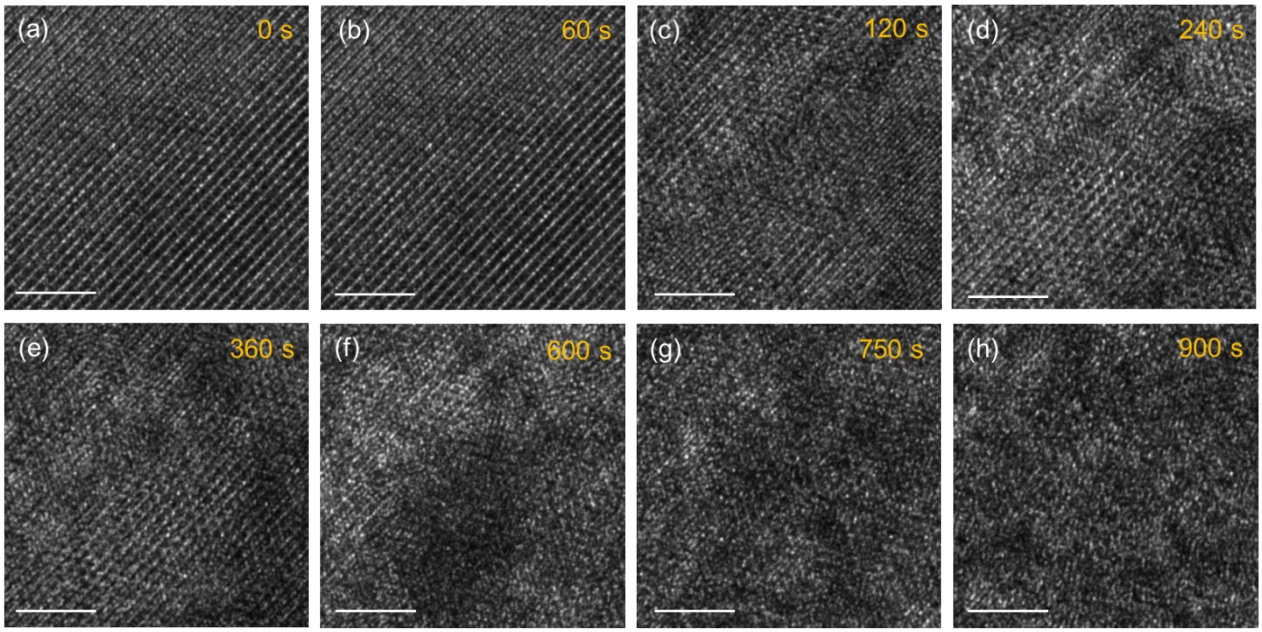

Fig. S2: Series of HRTEM images acquired at regular interval of time during electron beam irradiation depicting structural transformations in mixed metal oxide $W_{0.5}Mo_{0.5}O_3$; (Scale bar is 5 nm in all the panels).

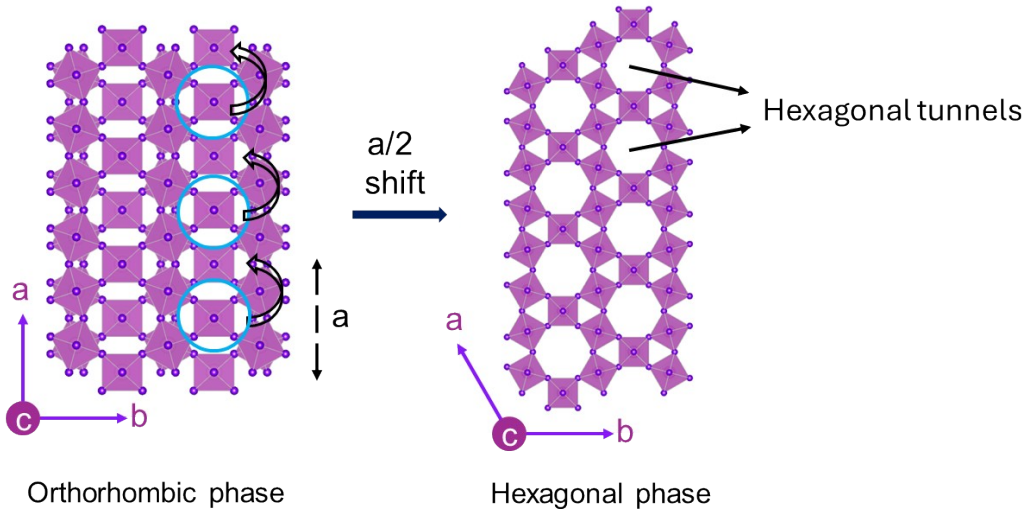

Fig. S3: Schematic depicting the plausible mechanism of orthorhombic to hexagonal phase transformation through atomic-model during electron-beam irradiation.

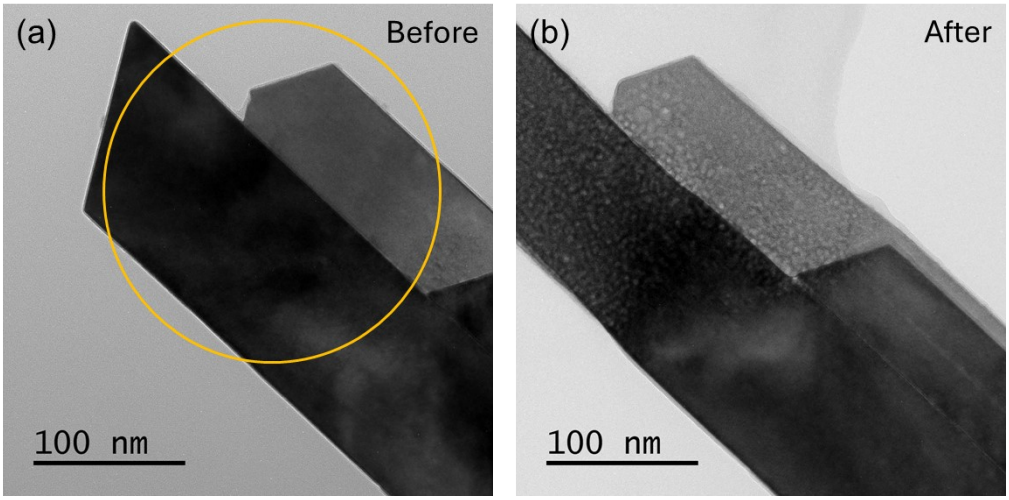

Fig. S4: BF-TEM micrograph of the $Mo_{0.5}W_{0.5}O_3$ sample before **(a)** and after **(b)** electron beam irradiation experiment, showing structural degradation through continuous exposure of electron beam (enclosed area in yellow circle is area illuminated).

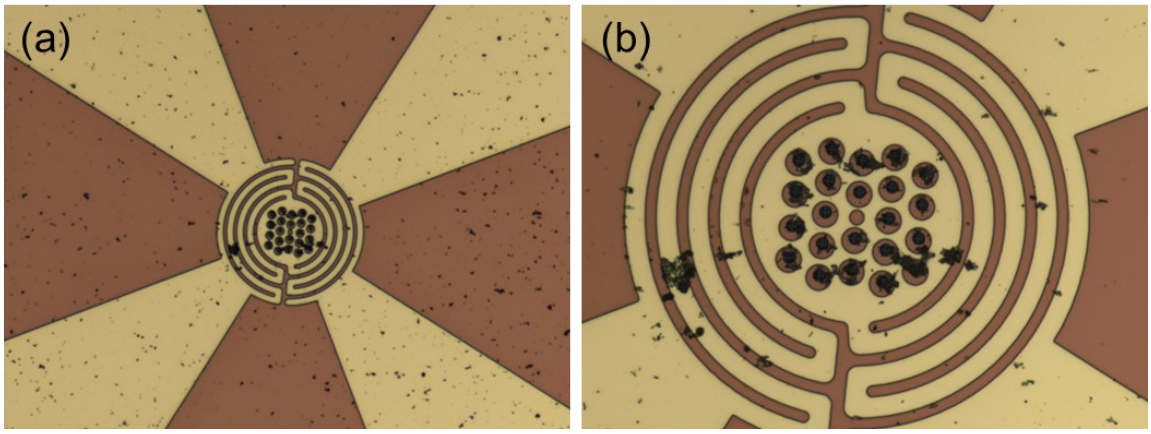

Fig. S5 (a-b): Light optical microscope images of $W_{0.5}Mo_{0.5}O_3$ sample (black contrast) drop casted on the viewing windows of MEMS chip for in-situ heating in TEM.

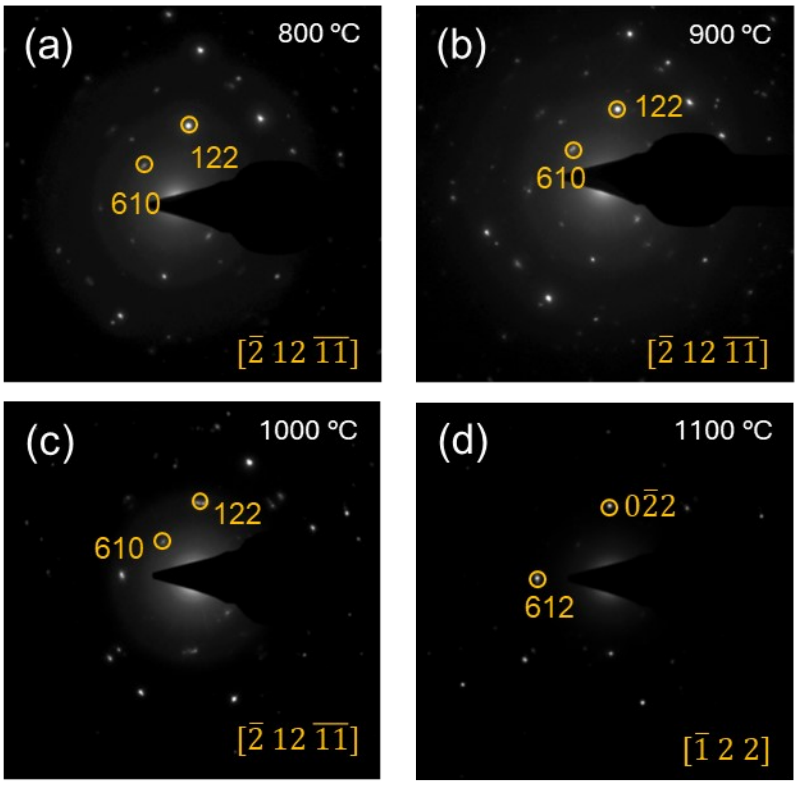

Fig. S6(a-d): SAED patterns of the mixed metal oxide taken during in-situ heating experiment after an interval of 100 °C; showcasing the growth of Mo_4O_{11} phase and the maintenance of single crystallinity.

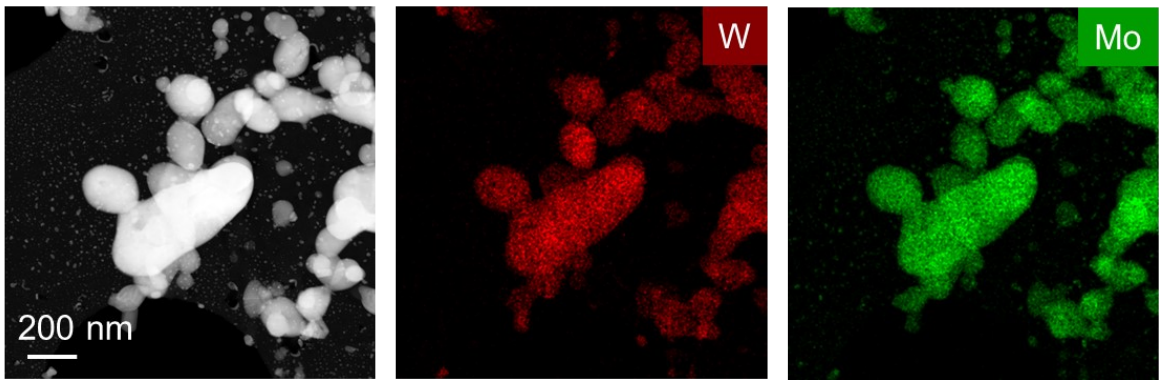

Fig. S7: STEM-EDS mapping of mixed metal oxide sample post in-situ TEM heating; showing preservation of uniform distribution of Mo and W even after 1200 °C with atomic fraction of 1:1.

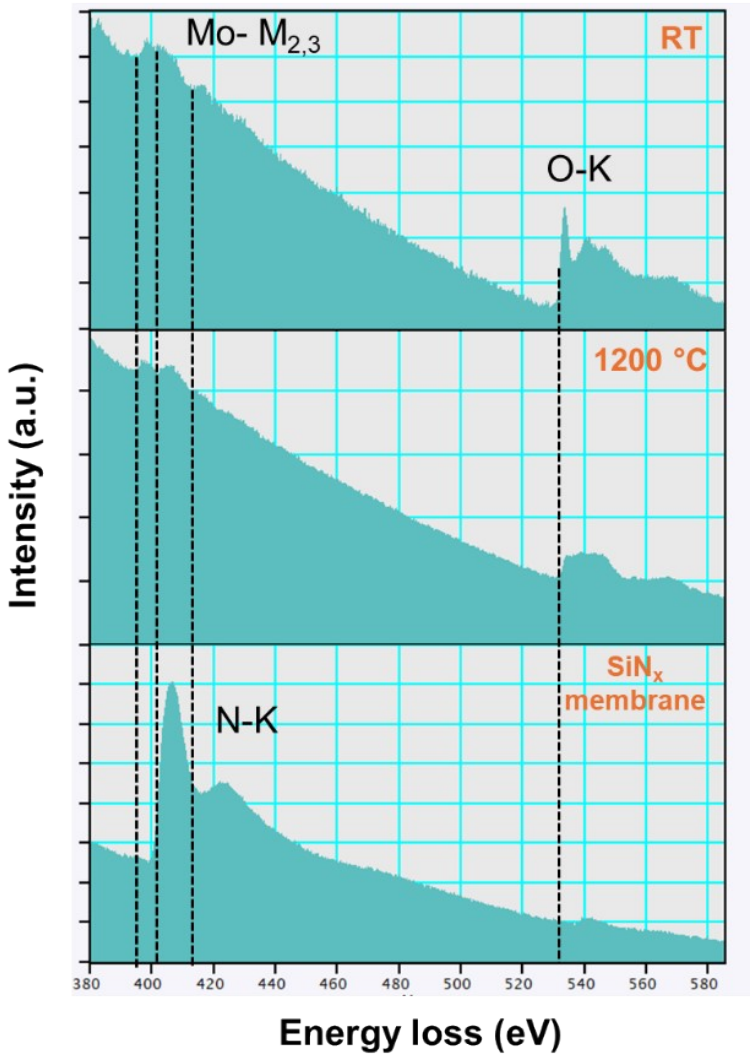

Fig. S8: EELS analysis of the sample before and after heating; Raw EELS data acquired in the energy-loss range of 380-580 eV for the sample at RT, 1200°C together with a reference spectrum from an empty SiN_x-MEMS chip at RT to cover the Mo $M_{2,3}$-edge and the O-K edge.

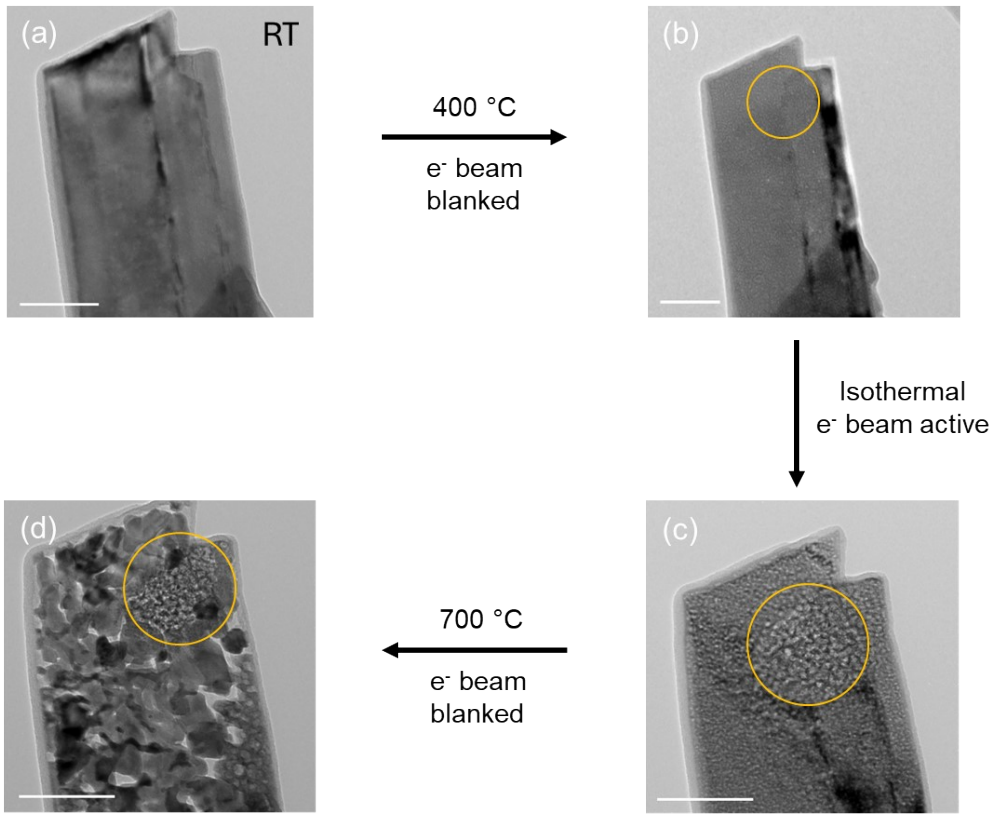

Fig. S9: Coupled thermal annealing and electron-beam irradiation effects in a single $Mo_{0.5}W_{0.5}O_3$ nanobelt; **(a-b)** TEM image acquired before and after 400 °C heating with the electron beam blanked; **(c)** TEM image acquired after 10 min of electron beam irradiation at 400 °C, showing localized structural degradation in the marked region; **(d)** TEM image acquired after further heating to 700 °C with the electron beam again blanked, demonstrating the phase transformation to oxygen-deficient $Mo_2W_2O_{11}$ throughout the nanobelt except within the previously irradiated region. Scale bar 100 nm in all panels.

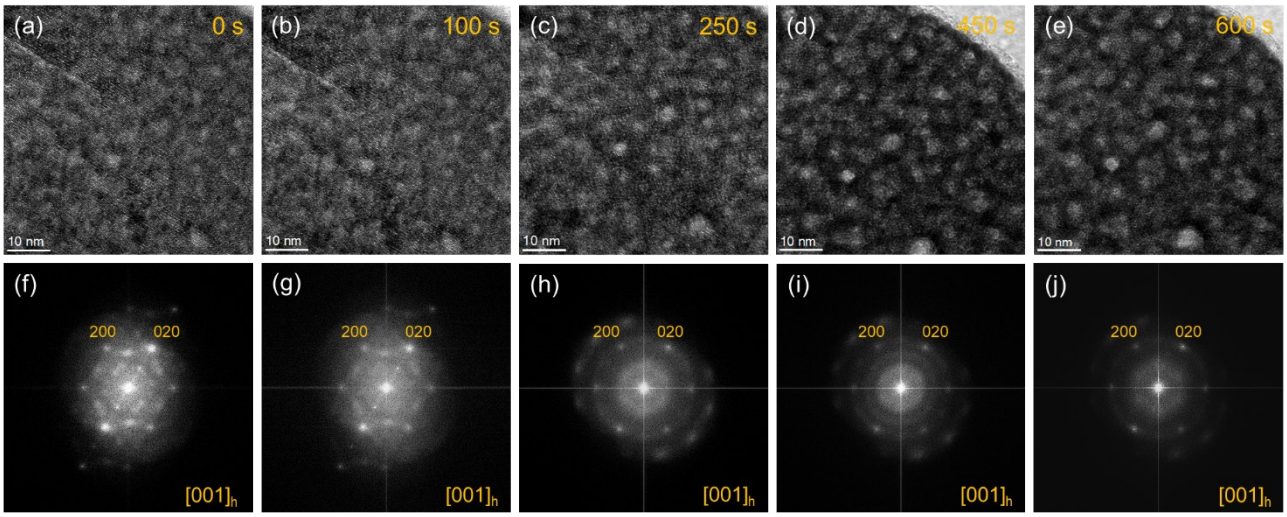

Fig. S10: Electron-beam irradiation effects in hexagonal $W_{0.5}Mo_{0.5}O_3$ formed during in situ thermal annealing at 400 °C under a constant dose rate of 2.5 × 10^6 e^- nm^{-2} s^{-1}; **(a-e)** HRTEM images acquired during continuous irradiation. **(f-j)** Corresponding FFTs showing progressive structural degradation, including loss in high-order symmetry and fading of diffraction spots.

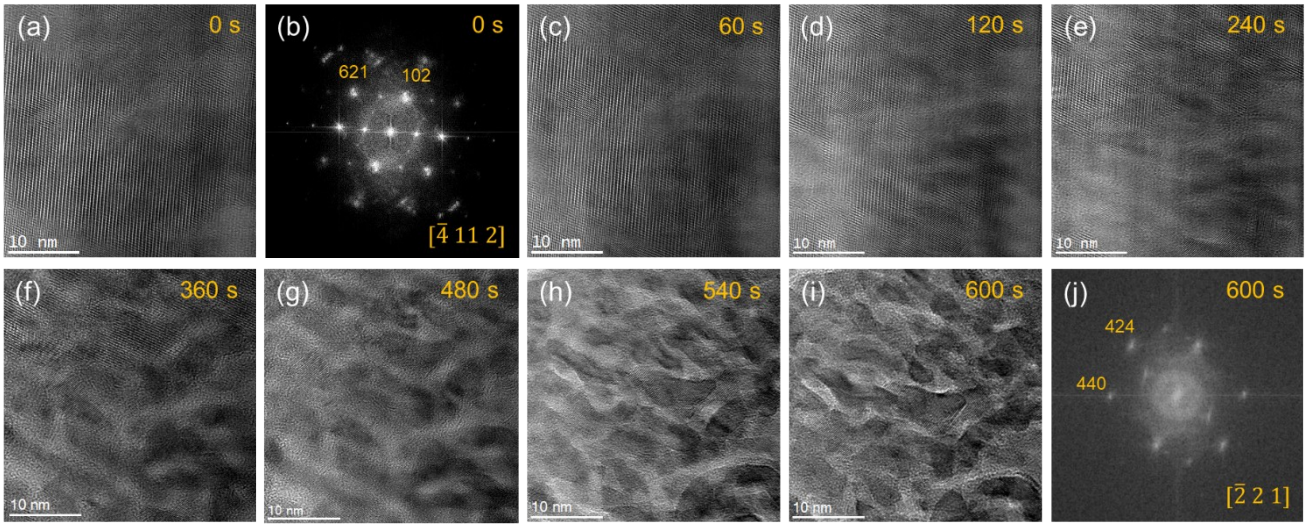

Fig. S11: Electron-beam irradiation effects in orthorhombic $Mo_2W_2O_{11}$ formed during in situ thermal annealing at 700 °C under a constant dose rate of 4.8 × 10^6 e^- nm^{-2} s^{-1}; **(a, c-i)** HRTEM images acquired during continuous irradiation. **(b,j)** Corresponding FFTs of (a) and (i), showing reduced crystallinity, loss of high-order symmetry, and fading of diffraction spots following prolonged electron-beam exposure.

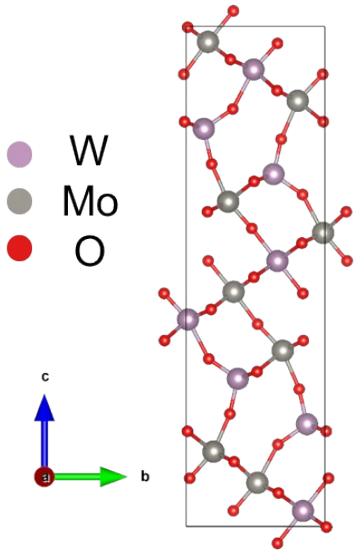

Fig. S12: DFT optimized structure model of $Mo_2W_2O_{11}$ formed by random substitution of half of Mo atoms from Mo_4O_{11} with W atoms.

References

1 G. Kresse and J. Hafner, *Phys. Rev. B*, 1993, **47**, 558–561.

2 A. Jain, S. P. Ong, G. Hautier, W. Chen, W. D. Richards, S. Dacek, S. Cholia, D. Gunter, D. Skinner, G. Ceder and K. A. Persson, *APL Mater.*, DOI:10.1063/1.4812323.

3 G. Kresse and D. Joubert, *Phys. Rev. B*, 1999, **59**, 1758–1775.

4 J. P. Perdew, K. Burke and M. Ernzerhof, *Phys. Rev. Lett.*, 1996, **77**, 3865–3868.

5 S. L. Dudarev, G. A. Botton, S. Y. Savrasov, C. J. Humphreys and A. P. Sutton, *Phys. Rev. B*, 1998, **57**, 1505–1509.